

# Supervised Saliency Map Driven Segmentation of the Lesions in Dermoscopic Images

Mostafa Jahanifar\*, Neda Zamani Tajeddin\*, *Student Member, IEEE*, Babak Mohammadzadeh Asl, and Ali Gooya, *Member, IEEE*

**Abstract**—Lesion segmentation is the first step in the most automatic melanoma recognition systems. There are some deficiencies and difficulties in dermoscopic images that make the lesion segmentation an intricate task e.g., hair occlusion, presence of dark corners and color charts, indistinct lesion borders, and lesions touching the image boundaries. In order to overcome these problems, we proposed a supervised saliency detection method specially tailored for dermoscopic images based on the discriminative regional feature integration (DRFI) method. DRFI method incorporates multi-level segmentation, regional contrast, property and backgroundness descriptors, and a random forest regressor to create saliency scores for each region in the image. In our improved saliency detection method, mDRFI, we have introduced some features as regional property descriptors and proposed a novel pseudo-background region to boost the performance. The overall segmentation framework uses the saliency map to construct an initial mask of the lesion through thresholding and post-processing operations. The initial mask is then evolving in a level set framework to fit better on the lesion’s boundaries. Results of evaluation experiments on three public datasets show that our proposed segmentation method outperforms the other conventional state-of-the-art segmentation algorithms and its performance is comparable with the most recent deep convolutional neural networks based approaches.

**Index Terms**—DRFI, ISBI challenges, skin lesion segmentation, supervised saliency detection.

## I. INTRODUCTION

NON-MELANOMA and melanoma skin cancers occurrence are both increasing in the recent decades. World Health Organization reports that the melanoma globally occurrence is about 132,000 each year, and by depleting the ozone levels this statistics will increase [1]. Fortunately, there is a high survival rate reported for melanoma as long as it diagnosed in early stages [2]. Computers and smart hand-held devices are very popular and pervasive these days and they can help to diagnose melanoma on time.

Lesion segmentation is the first step in the classical

Mostafa Jahanifar was with the Tarbiat Modares University, Tehran, Iran. He is now with the Department of Research and Development, NRP company, Tehran, Iran (e-mail: m.jahanifar@modares.ac.ir).

Neda Zamani Tajeddin and Babak Mohammadzadeh Asl are with the Biomedical Engineering Department, Tarbiat Modares University, Tehran, Iran (e-mails: {n.zamanitajeddin, babakmasl}@modares.ac.ir).

Ali Gooya is with the Department of Electronic and Electrical Engineering, University of Sheffield, Sheffield, England (e-mail: a.gooya@sheffield.ac.uk).

\*These authors contributed equally to this work.

computerized approaches of melanoma recognition systems [3]. Yu *et al.* [4] has shown that although classification of melanoma patients can be performed using only the features extracted by deep learning models, the diagnostic performance is elevated significantly by segmenting the lesions.

Different methods have been proposed in the literature for melanoma segmentation. Some researches segmented the lesion using thresholding and histogram analysis methods [5]–[7], some methods used only regional information [6], [8]. There are articles that took advantage of genetic algorithm and metaheuristic approaches [9], [10]. Hybrid methods that combine thresholding algorithms with the active contour models or level sets approaches were also exploited several times [3], [6], [11]. Recently, wavelet neural networks and convolutional neural networks proved to perform very well on dermoscopic image segmentation [4], [12]–[14].

Silveira *et al.* [6] assessed six different algorithms that were based on adaptive thresholding, active contours, levels sets, or regional information and they achieved the best results using adaptive snake algorithm [6]. Maglogiannis *et al.* [5] proposed a histogram based thresholding algorithm to segment the lesions from the background (healthy skin regions). Pennisi *et al.* [15] used Delaunay triangulation to partition the image into several regions and segment the lesion based on them. In our previous work [3] a histogram thresholding algorithm is used to achieve initial border of the lesion, which is then propagated towards the actual lesion boundary using a dual-component speed function in a level set framework.

In this paper, we proposed a similar approach to our previous work, however the initial mask of the lesion is constructed by thresholding the saliency map of the image. The contribution of this work relies on the construction of the saliency map. Based on prior information from dermoscopic images, we propose to integrate some new features into a well-known supervised saliency detection algorithm [16] framework in order to boost its performance on the lesion detection task. However, in the proposed method, constructed initial mask (achieved by processing the saliency map) is used in a level set framework to delineate the lesion’s boundary more precisely.

After reviewing related works, the rest of paper is organized as follow: in section II the supervised saliency detection algorithm is described. Our proposed segmentation method and the new added features are thoroughly explained in the section III. Results of applying the proposed methods on three

different datasets are reported in the section IV. In the section V we discuss the algorithm properties and performance and finally the paper is concluded in section VI.

#### A. Related saliency-based works

Salient object can be heuristically defined as the most prominent object in the image, region of the image that is noticed the first sight, or the segment of the image that has the most contrast from the background [17]. Salient object detection has been an active field of research in the recent years and there are many articles published on this topic. For a comprehensive review on saliency map creation methods please refer to [18]. Saliency object detection methods can be divided into two different groups: supervised, and unsupervised saliency detection mechanisms [18]. In the unsupervised manners, saliency map is created directly from image information and features. Most of these methods characterize the image contrast in different regions to obtain the saliency map. On the other hand for the supervised manner, like the approach we used in this paper, several features are extracted from the image’s regions and a predictor model which has been trained on a labeled dataset will construct the saliency map [16].

Lesion segmentation through saliency detection approaches has been addressed in the recent years [19], [20]. Fan *et al.* [19] proposed an unsupervised approach to construct two saliency scores, one from the image color information and the other one based on the image brightness information, and then create the final saliency map by combining these two saliency scores. Lesion segmentation is then achieved by thresholding the saliency map through a histogram analyzing method [19]. They used this priori information that the marginal area of the image belongs to healthy skin, which is not a true hypothesis all the times. They emphasized on the contrast property of lesion in the images and some lesion may have not enough contrast to fulfill their criteria. The other limitation of their algorithm is that they only used color and intensity information to construct saliency scores, which will not be enough for cases with color charts, because these charts show high contrast in the image and may be incorrectly detected as the lesion or the salient object.

Ahn *et al.* [10] first segmented the images into several superpixels and found the background regions using a multi-scale framework. After identifying the background regions they propose to create a saliency map via sparse reconstruction error. In other words, they claimed that the regions with larger reconstruction error are more likely to belong to the lesion [10] and used backgroundness of regions to detect the lesion. In the rest of their method they incorporate several saliency map refinements and a thresholding algorithm. Eventhough Ahn *et al.* [10] addressed the problem of lesions reaching to the boundary and achieve better results in comparison to [19], they were did not deal with color charts and dark corners in the images. Thus they simply removed these deficiencies manually before any processing, which is a tedious work.

In this paper, we propose a saliency detection method specially tailored for dermoscopic images which, not only uses

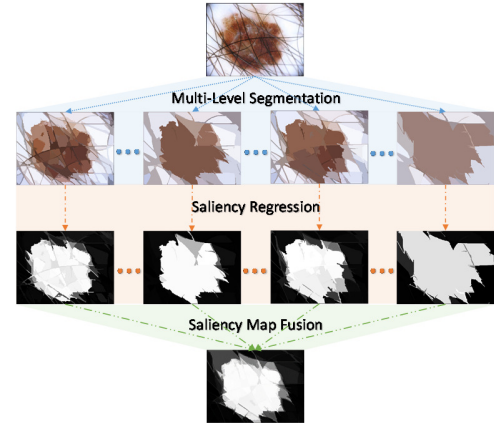


Fig. 1. DRFI saliency map detection procedure.

contrast and backgroundness descriptors, but also takes the location, shape, color, and texture information of the image regions into account to achieve a better result on saliency detection.

## II. SUPERVISED SALIENCY DETECTION

Assuming that lesion is a salient object in dermoscopic images, we proposed to use a saliency map construction algorithm to detect it. In this paper, likewise the work of Wang *et al.* [16], a multi-level segmentation scheme based on discriminative regional feature integration (DRFI) has been implemented. DRFI has been proven to be one of the most efficient algorithms for saliency detection based on the comprehensive experiments conducted in the recent benchmarks [17], [18].

In the supervised learning fashion of DRFI, a multi-level approach has been taken. First, the image is segmented into several regions at different levels and a saliency score is computed for the regions available in each level based on the regional information on that level. Saliency scores achieved from all levels are then combined to construct the final saliency map of the image. This supervised method benefits from a regressor model that constructs the saliency map from the regional feature vector. Main three steps of the Wang *et al.*’s DRFI algorithm [7] are listed below:

1. Multi-level segmentation: decomposition of the image to its constructing elements from a fine level to a coarse level.
2. Saliency regression: using a random forest regressor to map the regional feature vector into a saliency score.
3. Saliency map fusion: creating the final saliency map by fusing the saliency maps obtained from different levels.

A diagram of implemented saliency map construction algorithm and its outputs from different steps is shown for a sample image in Fig. 1. Each of the abovementioned steps has its own consideration, which we will explain briefly in the following subsections.

#### A. Multi-level segmentation

According to [16], in multi-level segmentation a graph-based image partitioning algorithm has been used [21]. The first level of segmentation (the finest) has the most number of output regions. The segmentation in the next levels is based on

TABLE I  
LIST OF REGIONAL CONTRAST AND BACKGROUNDNESS DESCRIPTORS

| features                                     | dimension |
|--|-----------|
| Average RGB values differences               | 3         |
| Average La*b* values differences             | 3         |
| Average HSV values                           | 3         |
| Absolute response of LM filters differences  | 15        |
| Max response among the LM filters difference | 1         |
| La*b* histogram difference                   | 1         |
| Hue histogram difference                     | 1         |
| Saturation histogram difference              | 1         |
| LBP histogram difference                     | 1         |

their previous levels of segmentation, which is done by merging adjacent similar regions. Thus the final level of segmentation (the coarsest) is likely to have the least number of regions. It is important to note that we are taking the relation of neighboring regions into account for saliency regression by working in a multi-level segmentation framework.

### B. Saliency regression for each level

In the second step of DRFI, regional features are extracted from each segmented regions (at different levels) of the image. There are three types of regional features in DRFI approach [16]: regional contrast, regional property and regional backgroundness.

#### 1) Regional contrast descriptors

Wang *et al.* [16] proposed to extract features representing the regional contrast and use them alongside the regional property and the backgroundness descriptor to elevate the quality of saliency detection. To compute the contrast descriptors, features from each region are compared with the features extracted from their neighboring regions.

In a specific segmentation level, different features can be extracted from its regions, which we will notate as regional feature vector  $v^R$ . Also, considering all adjacent regions as a single region, we can extract the same features from the neighboring region and construct the neighborhood feature vector  $v^N$ . To measure each region contrast descriptor, DRFI method proposes to calculate the difference of  $v^R$  and  $v^N$  as follow:

$$d(v^R, v^N) = \begin{cases} \sum_{i=1}^b \frac{2(v_i^R - v_i^N)^2}{v_i^R + v_i^N}; & \text{for histograms} \\ (|v_1^R - v_1^N|, \dots, |v_d^R - v_d^N|); & \text{O.W.} \end{cases}, \quad (1)$$

meaning that for features that comprise a histogram a normalized sum of histogram bins are considered to be the feature differences, and for other features it is calculated as the absolute element wise difference. Wang’s proposed feature set for contrast description is summarized in Table I [16].

Here we address items in Table I which were not described in [16]. The third and fourth items in the Table I correspond to the response of image to the kernels of Leung-Malik (LM) filter bank [22]. In DRFI a subset of LM filter bank consists of

TABLE II  
LIST OF REGIONAL PROPERTY DESCRIPTORS

| features  | dimension |
|---|-----------|
| Average normalized x and y coordinates  | 2         |
| 10 <sup>th</sup> and 90 <sup>th</sup> percentiles of normalized x and y coordinates | 4         |
| Normalized area and perimeter   | 2         |
| Normalized area of neighboring regions  | 1         |
| Aspect ratio of bounding box  | 1         |
| Variance of the RGB values  | 3         |
| Variance of the La*b* values  | 3         |
| Variance of the HSV values  | 3         |
| Variance of the response of the LM filters  | 15        |
| Variance of LBP feature   | 1         |
| <b>Average of the RGB values</b>  | <b>3</b>  |
| <b>Average of the a* and b* values (from La*b*)</b>                                 | <b>2</b>  |
| <b>Shape elongation</b>   | <b>1</b>  |
| <b>Shape extent</b>   | <b>1</b>  |
| <b>Circle probability</b>   | <b>1</b>  |
| <b>Energy of Laws’ filters responses</b>  | <b>14</b> |
| <b>Segmentation level</b>   | <b>1</b>  |

Bold faced items are newly introduced in this work.

the first and the second derivatives of Gaussian kernel (each at 6 different orientations), 1 Gaussian kernel, and 2 Laplacian of Gaussian kernels (these kernels are illustrated in Fig. 5). First, image is convolved with each of LM filters and then the average of the convolution responses in each region is calculated to serve as a texture descriptor. The maximum response among LM filters responses is detected and its histogram for each region pixels is also considered as a texture descriptor. The last item in Table I refers to the histogram of the local binary pattern (LBP) [23] of the image. To compute that, the LBP of the image is extracted and then for each region the histogram of LBP is constructed to represent that region texture. It is important to remind that the items in Table I are the differences of features in each region from their neighboring regions.

#### 2) Regional property descriptors

This group of features directly describe the shape, location, color, or texture of the regions. These features can be very useful when contract descriptors are impractical. For example, in a dermoscopic image a color chart indicator with green color shows a great contrast against the healthy skin, whereas it is not an eligible salient object that we are seeking. Thus, the contrast descriptor alone cannot work very well here. Fortunately, regressor in DRFI method can easily be trained to neglect green regions in the image by adding some regional descriptors in the training phase, even though that region has high contrast. Wang *et al.* [16] proposed 35 regional property features for DRFI that are listed in Table II (with regular font).

#### 3) Regional backgroundness descriptors

It has been shown that region properties cannot identify the background in natural images [16], [17]. By assuming this hypothesis that most of the salient objects are placed in the center of the image, DRFI considers a pseudo-background region to calculate the degree of backgroundness of other regions based on it. In [6], a border of 15 pixels around the

image area has been picked out as the pseudo-background regions. Just like regional contrast descriptors, DRFI proposes to calculate the difference of each region’s features from the features of the pseudo-background region to serve as the regional backgroundness descriptors.

#### 4) Saliency regression

By combining the contrast, property, and backgroundness descriptors for a region, a regional feature vector will be formed to describe that region. The feature vector is extracted from each segment of the image in every levels. For a dataset consisting of images and the manual segmentation of salient object, we can train a regressor to learn regional features and predict saliency scores as follows.

For each level in the multi-level segmentation framework, regional feature vectors should be extracted for all regions of that level. The corresponding labels (whether a region belongs to the salient object: 1 or not: 0) for each region are also available through their ground truth segmentation mask. Regional feature and label vectors are then utilized to train a random forest regressor [24]. In the prediction phase, the trained regressor gets the saliency feature vector for a region and returns a saliency score between 0 and 1. By predicting the saliency scores for all regions in an image (for a certain level), its saliency map is constructed.

#### C. Saliency map fusion

To achieve the final saliency map, saliency maps of different levels must be fused. Based on [6], a linear combinator has been implemented for this task. This combinator constructs the final saliency map by operating a weighted integration of multi-level saliency maps. DRFI learns the combination weights through the least square method on the training images [6].

### III. PROPOSED SEGMENTATION METHOD

For segmenting the lesion in dermoscopic images we will follow the method illustrated in the diagram of the Fig. 1. Proposed segmentation method consists of three main parts: preprocessing, initial mask creation, and final mask creation. The preprocessing steps aim to compensate for the deficiencies in the image, like hair occlusion or color inconstancy. The goal of the second part of the algorithm is to construct an initial mask for the lesion, this mask will further be used in the third part of the algorithm to better delineate lesion border in the image. Each of these parts consists of different algorithmic steps, which will be described in the next subsections.

#### A. Preprocessing

Due to different deficiencies that usually exist in the dermoscopic images, preprocessing is a vital task before any further analysis. The most problematic issues in the image can be hair occlusion, uneven illumination, color inconstancy, ruler marks, color charts, and dark corners [25]. Lesion segmentation could undergo some difficulties because of these deficiencies. Likely, we can reduce their destructive effects by applying preprocessing techniques. There are vast variety of

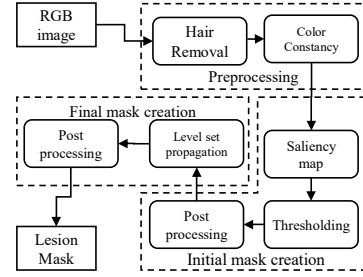


Fig. 2. An overview diagram of the proposed segmentation method.

methods proposed to solve each of these problems [2, 9, 10]. Because we are planning to segment the lesion in a supervised learning framework, we suppose that such algorithms should be able to distinguish color charts or dark corners from the lesion. Therefore, unlike the approaches we took in our earlier work [3], in this paper we only explore the effects of hair removal and color constancy on image segmentation.

#### 1) Color constancy

A general dataset of dermoscopic images, like the one in ISBI 2017 challenge, comprises of images captured in different lighting situations using different dermoscope devices. Based on this fact, image color would change from image to image which will lower the performance of learning algorithms [26]. Here we proposed to use color constancy to reduce color variation in dataset images using shades of gray algorithm described in [26]. Shades of gray proposes to correct each channel in the image based on that channel weighted norm  $e_c$  calculated using (2), in which  $I_c$  is one of the image channels  $c \in \{R, G, B\}$  on the image domain  $\mathbf{x}$ ,  $k$  is a normalization constant, and  $p$  is the norm degree [26]:

$$e_c = \frac{1}{k} \left( \frac{\int (I_c(\mathbf{x}))^p d\mathbf{x}}{\int d\mathbf{x}} \right)^{1/p} \quad (2)$$

Based on the above equation, the normalization constant  $k$  can be computed by setting  $\sqrt{e_R^2 + e_G^2 + e_B^2} = 1$ . Finally, correction coefficient for each channel is calculated as  $d_c = (\sqrt{3}e_c)^{-1}$ . By multiplying each correction coefficient in its corresponding image channel, the color corrected image can be achieved. As in the work of Barata *et al.* [26], the parameter  $p$  was set to 6. The result of applying such algorithm on a sample dermoscopic image, occluded with hairs and has a shade of blue in its color, is illustrated in Fig. 3. Applying the color constancy seems to improve the contrast of the lesion in comparison to the surrounding skin, also, the range of colors becomes more consistent with the other images in the dataset.

#### 2) Hair and ruler marks inpainting

Hair occlusion can jeopardize the segmentation task. In this paper we used the method described in [27] to detect hair like structures in the image and replace them with appropriate pixel values. Koehoorn *et al.* [27] proposed a multi-threshold scheme to initially segment the hairs in the image. In every thresholding step, they used gap-detection algorithm to detect

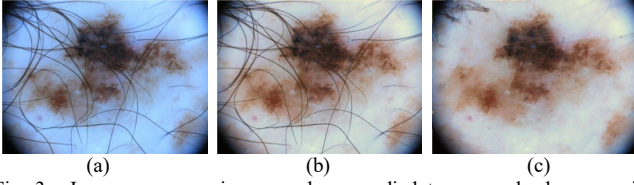


Fig. 3. Image preprocessing procedures applied to a sample dermoscopic image: (a) original image occluded with hairs and showing a shade of blue color, (b) applying shade of gray algorithm to achieve color constancy, and (c) removing hair from the color corrected image using Koehn's method [27].

potentially hair pixels. All initial results are then combined into a single mask. This mask contains some objects that are falsely segmented as hair. Thus, in the last step of algorithm authors used a combination of morphological filters and medial descriptors to validate the hair objects. Detected hair pixels are then replaced using a fast marching based image inpainting algorithm [27]. This approach is capable of detecting and inpainting dark and light hairs from the image.

### B. Initial mask creation through saliency detection

Considering the lesion as the salient object in dermoscopic images, we propose to use the supervised saliency detection method explained in the section II for lesion detection. DRFI approach originally introduced by Wang *et al.* [6] has been designed to detect salient objects in dataset of natural images, which are very challenging. Dermoscopic images, on the other hand, have their own challenges that must be considered in the saliency detection pipeline. Knowing specific properties about dermoscopic images helps us to extend DRFI feature set to better describe them. Accordingly, in this section we propose to improve the DRFI approach by incorporating new regional property descriptors and a more relevant pseudo-background region in its framework. Apart from these novelties, all other procedures for saliency detection are followed as described in section II.

#### 1) Modifying DRFI for dermoscopic saliency detection

To improve the performance of DRFI approach on dermoscopic images, we proposed to extend the regional property descriptors and introduced a new pseudo-background region that specifies the healthy skin regions only. This new modified version of DRFI is the key contribution in this paper and we abbreviate it “mDRFI” in the rest of paper.

##### 1.1) Extending regional property descriptors

It has been shown that the regional property descriptors have a great impact on the saliency regression (based on experiments on natural image datasets, 9 features out of 20 most important regional features belong to this group) [6]. We propose to add the following features to the regional property descriptors of mDRFI in order to improve its functionality for detecting skin lesions as the salient object. Newly added features can be categorized in color, shape, or texture related features.

*Color related features:* in the original DRFI approach, the variance of region pixel values from different color channels (R, G, B, L, a\*, b\*, H, S, and V) have been used as the regional property descriptor. Variance of pixel values is a texture descriptor which measures the amount of changes in a region appearance. To capture the color properties of a region,

we propose to extract the average of R, G, B, a\*, and b\* channels in that region as the absolute color descriptors (5 new regional property features added to mDRFI).

*Shape related feature:* some structures in the image can be identified via their shape. Hairs in dermoscopic images are tubular structures which usually have long and thin shapes. We are able to characterize this property of a region by adding a feature that measures the shape elongation:

$$\text{Elongation} = 1 - m/M, \quad (3)$$

where  $m$  and  $M$  are the lengths of the minor and major axes of the ellipse that has the same normalized second central moments as the region. We also propose to add a feature measuring the extent of the region to describe rectangularity of its shape. The extent is calculated by dividing the region area by the area of its bounding box.

It is very important not to confuse the color charts around some images as the salient object. Some of these charts can easily be recognized by their color (e.g., pure green color chart), but it is common for color charts to have similar colors to lesions. Ergo, it is vital to use their shape and position properties to recognize them and preventing regressor to wrongly detect them as the salient object. For this end, we have employed the method of Basalmah [28] for partial circle detection.

Edge map,  $\Omega$ , of the image is constructed by thresholding the Prewitt gradient of the image. Then, for each pixel of the image,  $(x, y)$ , the Euclidean distance to every edge pixel,  $(i, j) \in \{\Omega = 1\}$ , in the edge map is collected in a distance vector,  $\mathbf{dist}_{(x,y)} = \{\text{dist}_{(x,y)}^{(i,j)}, (i, j) \in \{\Omega = 1\}\}$ , in which distance function is defined as Euclidean distance:

$$\text{dist}_{(x,y)}^{(i,j)} = \sqrt{(i-x)^2 + (j-y)^2}. \quad (4)$$

The histogram of that distance vector for each pixel location,  $\mathbf{H}_{(x,y)}$ , is constructed to be used in further analysis and finding the potentially circles:

$$\mathbf{H}_{(x,y)} = \{h_{(x,y)}^d; d = 0, \dots, D\}, \text{ in which:} \quad (5)$$

$$h_{(x,y)}^d = \#\{(i, j) \in \Omega \mid \exists \text{dist}_{(x,y)}^{(i,j)} = d\}.$$

We form a *centerMap* and a *radiusMap* with the same size as the original image and for each pixel the maximum values of its histogram are recorded in that pixel position in the *centerMap*. The location of histogram maximum is also recorded in the same pixel position of *radiusMap*:

$$\text{centerMap}(x, y) = \max(\mathbf{H}_{(x,y)}), \quad (6)$$

$$\text{radiusMap}(x, y) = \underset{d}{\text{argmax}}(\mathbf{H}_{(x,y)}).$$

Dominant peaks (peaks greater than a threshold) indicate that the pixels under investigation can be the center of a circle, because they have a great number of edge pixels distributed with equal distance around them. Thus, we convert the *centerMap* to a binary mask which indicates the location of circles' center by applying a domination threshold on it. Values of the *radiusMap* in the location of centers also



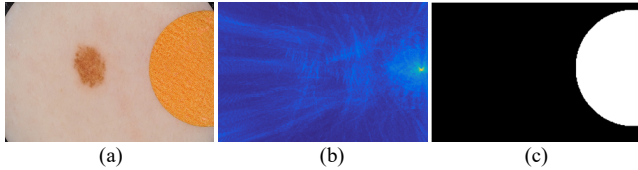


Fig. 4. Procedure of circle detection for construction of the circle probability map: image (a) is the original input to the algorithm, (b) is the *centerMap* showing high values near the circle's center location, and (c) is obtained circle probability map (detected circle mask).

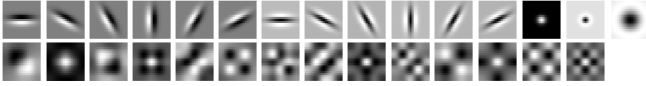


Fig. 5. Top row shows 15 kernels of LM filter bank. The bottom row illustrates 14 Laws' filters which are able to enhance more complex templates.

indicate their corresponding circle radius. Having the circle's center position and its radius, we can construct a probability map of circles for the image (we add this to regional property descriptors under the name of *circle probability*). Intermediate results of applying such method on a sample image are demonstrated in Fig. 4. In the image Fig. 4-(a), the color chart has almost the same color as the lesion, so it is not feasible to recognize its region via its absolute color descriptors. But, using the proposed partial circle detection algorithm, we were able to identify the color chart at the margin of the image Fig. 4-(c). Hitherto, 3 new shape features are added to regional property descriptors of mDRFI.

*Texture related features:* other than low level texture descriptors like variance of pixel values, DRFI used the responses of LM filters to represent regions' texture properties. As illustrated in Fig. 5, LM filters mostly emphasis on tubular and spot like structures. To enhance and represent more complicated texture templates in the image, we propose to add the responses of Law's filter bank to the mDRFI as well. Laws' energy features (LEFs) emphasizes on edge, spot, ripple, and wave structures in the texture of the image. Each of Laws' texture descriptors is defined based on the following five basic operators [29]:

$$\begin{aligned}
 \text{Average} = L_5 &= [1, 4, 6, 4, 1], \\
 \text{Edge} = E_5 &= [-1, -2, 0, 2, 1], \\
 \text{Spot} = S_5 &= [-1, 0, 2, 0, -1], \\
 \text{Ripple} = R_5 &= [1, -4, 6, -4, 1], \\
 \text{Wave} = W_5 &= [-1, 2, 0, -2, 1].
 \end{aligned} \tag{7}$$

By combining these five operators with each other (through matrix multiplication), 14 different Law's descriptors can be obtained (list of all descriptors can be found in [45]), their corresponding visualization are illustrated in Fig. 5. As one can see in Fig. 5, each descriptor targets a specific textural structure.

Each of Laws' descriptors can be convolved with the image and act as a filter to enhance specific features in the image. We use this property to represent lesion's texture. After filtering the lesion image with each of fourteen Law's descriptors, we obtain fourteen filter responses, where in each of them, a particular textural structure is highlighted. We compute the energy of pixels belonging to each regions from filter responses to construct a textural feature descriptor. We

have fourteen filter responses, so we would have 14 different filter response energies, which can be used as texture features (14 new regional property features added to mDRFI).

In summary, we have added 3 shape (elongation, extent, and circle probability), 5 color (average of R, G, B,  $a^*$ , and  $b^*$ ), and 14 texture (energy of Laws' filters responses) features to mDRFI. In addition to that, we propose to consider the segmentation level as an input feature to the random forest regressor as well. In total, we have extended the regional property descriptors of mDRFI by 23 new features, which are listed in the Table II with bold faces.

### 1.2) New pseudo-background region

In dermoscopic images, healthy skin around the lesion can be assumed to be background [10]. It is necessary to correctly specify the background region before any attempt to extract regional backgroundness descriptors. It is known that for some images in a general dermoscopic dataset, such as ISBI2017, there are some images that include other objects (like color charts or dark corners) in their marginal area. More importantly, some lesions extents reach the image borders. Therefore, that marginal regions should not be considered as background. To eliminate undesired effects of these problems, we introduced a new pseudo-background region.

To extract it, first we compute the histogram of the image and then smoothed it by applying a moving average filter. We find the location of the last peak in the histogram and set its 90<sup>th</sup> percentile as the background threshold to convert the image into a binary mask of background. After that, we apply some post processing operations (filling holes, removing small objects, and morphological closing) on the output background mask. Finally, a margin of 15 pixels starting from the outer boundary of the background object toward its inside is selected as the pseudo-background region. Fig. 6 shows the output of this procedure for a sample dermoscopic image that has both dark corners and lesion touching the borders. It is desirable that the pseudo-background region only encompasses the healthy skin, as our proposed algorithm finds it in Fig. 6-(e).

### 2) Thresholding the saliency map

Binary mask of the lesion is achieved by thresholding the output saliency map of mDRFI method. Constant threshold of 0.5 has been used to convert the saliency maps to binary masks. Of course, the binary mask has spurious parts in it which makes it unacceptable to be the lesion's initial mask. These are removed by steps taken below.

### 3) Post processing (initial mask)

To make the binary mask more appropriate for the next segmentation part, we applied some post processing tasks on it. First, an analysis of objects area is carried out. The average area ( $a_m$ ) and standard deviation ( $a_s$ ) of objects' areas are calculated and then objects with areas smaller that  $a_m - 2a_s$  were removed from the binary mask. Convex hull of the remaining objects is then constructed to serve as the initial mask of the lesion.

### C. Final mask creation

The initial mask may not represent the boundary of the

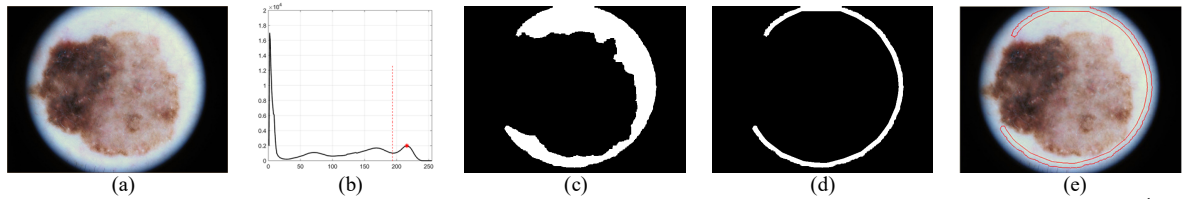


Fig. 6. Obtaining new pseudo-background region: (a) original image, (b) histogram of the gray image, in which the last peak is found and the 90<sup>th</sup> percentile of its location is selected as threshold, (c) thresholded and processed mask of background, (d) and (e) represent the new pseudo-background region.

lesion perfectly. We propose to further refine the initial segmentation through level set evolution. We have used the signed distance function of the initial mask as the initial state of level set in a distance regularized level set evolution (DRLSE) framework [30] to drive it toward the lesion boundary. Image channel with the highest entropy has been chosen [6] to be used in DRLSE framework. After level set evolution, we applied some post processing tasks (morphological opening and closing) on the DRLSE output to smooth out its boundary and improve the results.

#### IV. EXPERIMENTAL SETUP AND RESULTS

##### A. Datasets description

To evaluate our mDRFI approach and the proposed segmentation method, we used three different datasets. Two of these datasets are selected from international skin imaging collaboration (ISIC) archive that have been used in the challenge of “Skin Lesion Analysis toward Melanoma Detection” [31] held by international symposium on biomedical imaging (ISBI) in two years of 2016 and 2017, which abbreviated here as ISBI2016 and ISBI2017, respectively. Parts of the ISBI2016 dataset that we have used in this article comprise of 900 and 397 images for training and testing, respectively. The ISBI2017 dataset also comprises 2000 images for training, 600 images as testing set. Images in ISBI2016 and ISBI2017 have a great number of duplicate items, so we will train and test our algorithm on each of these dataset separately. Another dataset that has been widely used in the field of dermoscopic image analysis is PH2 dataset [32] which comprises total of 200 dermoscopic images. Images have been captured in different resolutions, so we resize them to a mutual size of 300×400 before any processing.

##### B. Implementation details

Codes have been implemented in MATLAB R2014b, and all experiments were performed on an Intel Core i7-4790 machine with 16 GB memory running Ubuntu. Hair removal has been done using GPU implementation of Koehoorn algorithm<sup>1</sup> [27]. Our implementation of mDRFI has been released<sup>2</sup>, which consist of the implementation of image color constancy correction and all other novelties alongside the original DRFI source code. DRLSE toolbox for level set evolution is available online<sup>3</sup>, as well.

##### C. Quantitative and qualitative results

To evaluate the segmentation algorithms quantitatively, we have incorporated Disc Similarity Coefficient (DSC) and Jaccard Similarity Index (JSI), and three pixel-wise performance metrics of Accuracy (Acc), Sensitivity (Sens), and Specificity (Spec) as described in [31]. Results of experimenting the proposed segmentation algorithm on different dermoscopic datasets in comparison to the results of the other state-of-the-art methods are reported in Tables III-VII. Some evaluation metrics are absent for some methods, so we replace their corresponding values by “-” character in our reported tables.

For PH2 dataset in Table III, our algorithm outperforms the other reported researches. It is worth mentioning that method of Silveira *et al.* [6] is a semi-automatic method that needs user to select a region inside and outside of the lesion. PH2 is relatively small and simple dataset that all of its images have been captured using a fixed acquisition setup, so it is rational to achieve evaluation metrics as high as reported in Table III.

For ISBI2016 dataset, results are reported for both training and testing sets. For the training set in Table IV, our algorithm outperforms the other saliency detection based algorithms (Fan *et al.* [19] and Ahn *et al.* [20]) and our previous method in Zamani *et al.* [3], but its performance reported to be a slightly worse than that of Yuan *et al.* [14] method, which is based on deep convolutional neural networks (DCNNs). Evaluation on ISBI2016 test set is also reported in Table V. Based on this table our algorithm performance is listed within top 3 algorithms and outperforms other methods that ranking 2 to 5 at the ISBI2016 Part 1: Segmentation challenge (including our previous method named “TMUteam” [3]).

In the same way, we applied our method on ISBI2017 train and test set and reported the results in Table VI and Table VII, respectively. Our proposed algorithm ranked 7<sup>th</sup> among 21 teams competing in the “Part 1: Lesion Segmentation” of the “ISBI 2017 Skin Lesion Analysis Towards Melanoma Detection” with insignificant differences from the other superior methods. Algorithm proposed in Yuan *et al.* [14] ranked first place in lesion segmentation, again. Our proposed algorithm achieved average Dice value of 0.839 and Jaccard index of 0.749 on 600 images of ISBI2017 test set, which only are respectively 0.010 and 0.015 lesser than Dice and Jaccard values reported for the first ranked method (Yading Yuan). Differences from results of the other superior competitors in the Table VII are even smaller (other evaluation metrics have the same trend). These results prove the confidence of the proposed segmentation algorithm in comparison with the other state-of-the-art methods, which mostly are based on DCNNs.

<sup>1</sup> Code provided at: <http://www.cs.rug.nl/svcg/Shapes/HairRemoval>

<sup>2</sup> Code released at: [https://github.com/mjahhanifar/mDRFI\\_matlab](https://github.com/mjahhanifar/mDRFI_matlab)

<sup>3</sup> Code available at: <http://www.imagecomputing.org/~cml/DRLSE/>

In order to assess the proposed segmentation algorithm qualitatively, we have employed it on several extreme cases of dermoscopic images and illustrated the resulting outputs in Fig. 7. The output saliency maps from mDRFI method are also shown for each sample under it. In each image of Fig. 7, the green contours represent the ground truth segmentation, red dashed lines stand for the contour of the lesion’s initial mask (constructed by thresholding the saliency map as explained in the section III-B), and the blue contours show the borders of the refined final segmentation through level set evolution (as described in the section III-C).

## V. DISCUSSION

### A. mDRFI optimal parameter selection

In mDRFI, like original DRFI, saliency map detection depends on some parameters. The most important parameters that should be explored are the number of segmentation levels in the multi-level framework and the number of trees in the random forest regressor [6]. To find the optimal ranges for these parameters, we split the ISBI2017 training set into two subsets: a train subset with 1500 images and a validation subset comprising 500 images. First, we set the number of trees to a constant number of 150 and train mDRFI models with different number of segmentation levels on the training subset and use them to predict saliency maps on the validation subset. The average values of AUC (area under ROC curves) obtained from evaluation of 200 saliency maps are then reported for each mDRFI configuration. As shown in Fig. 8-(a), increasing the number of segmentation levels would elevate the mDRFI performance, because increasing the number of segmentation levels may form some confident regions that cover more areas of the lesion [6]. Based on this experiment of the AUC curve in Fig. 8-(a), we have decided to set the number of segmentations equal to 15 in this work.

The same experiment has been carried out to assess the different number of trees in the random forest regressor. It has been proved that increasing the number of trees would decrease the variances within the weak classifiers of the random forest regressor and lead to a better performance [6]. Considering the efficiency and computational load trade off, we selected the number of trees to be equal to 200 based on the validation experiment in Fig. 8-(b).

Although we have selected the optimal parameters for training mDRFI, plots in Fig. 8 show a small variation for AUC scores by changing the parameters e.g., by changing the number of segmentation from 1 to 25 the performance metric (AUC) varies only about 0.012 (1%). This implies that proposed mDRFI approach has a low sensitivity to parameter selection.

### B. Exploring the effect of preprocessing

In order to trace the effect of the preprocessing tasks on the mDRFI performance, the ROC (receiver operating characteristic) curve has been employed [18] in the following procedure. We have trained the mDRFI model on the ISBI2016 train set images and predicted the saliency maps of

TABLE III  
RESULTS OF PH<sup>2</sup> DATASET SEGMENTATIONS

| Method          | Average of evaluation metrics (%) |      |      |      |      |
|-----------------|-----------------------------------|------|------|------|------|
|                 | DSC                               | JSI  | Acc  | Sens | Spec |
| Silveira [6]    | 94.0                              | -    | -    | 97.0 | 96.0 |
| Pennisi [15]    | -                                 | -    | 89.4 | 71.0 | 97.1 |
| Maglogianis [5] | 90.0                              | 83.7 | 92.8 | 90.4 | 97.0 |
| Ahn [20]        | 91.5                              | -    | -    | -    | -    |
| Fan [19]        | 89.3                              | -    | 93.6 | 87.0 | -    |
| Zamani [3]      | 92.0                              | 85.8 | 96.5 | 95.4 | 98.1 |
| Proposed        | 95.2                              | 92.3 | 97.9 | 97.2 | 98.9 |

TABLE IV  
RESULTS OF ISBI2016 TRAIN SET SEGMENTATIONS

| Method     | Average of evaluation metrics (%) |      |      |      |      |
|------------|-----------------------------------|------|------|------|------|
|            | DSC                               | JSI  | Acc  | Sens | Spec |
| Fan [19]   | 81.8                              | -    | 91.8 | 74.7 | -    |
| Ahn [20]   | 83.9                              | -    | -    | -    | -    |
| Zamani [3] | 89.5                              | 80.2 | 93.5 | 83.2 | 98.7 |
| Proposed   | 91.7                              | 85.5 | 94.2 | 88.7 | 98.4 |
| Yuan [14]  | 92.2                              | 86.1 | 96.3 | 92.6 | 97.1 |

TABLE V  
RESULTS OF ISBI2016 TEST SET SEGMENTATIONS  
(ADOPTED DIRECTLY FROM THE ISBI2016 CHALLENGE WEBSITE\*)

| Method                  | Average of evaluation metrics (%) |      |      |      |      |
|-------------------------|-----------------------------------|------|------|------|------|
|                         | DSC                               | JSI  | Acc  | Sens | Spec |
| Yuan [14]               | 91.2                              | 87.4 | 95.5 | 91.8 | 96.6 |
| Proposed                | 90.7                              | 83.8 | 94.3 | 90.1 | 98.2 |
| 1) EXB                  | 91.0                              | 84.3 | 95.3 | 91.0 | 96.5 |
| 2) CUMED (Yu [4])       | 89.7                              | 82.9 | 94.9 | 91.1 | 95.7 |
| 3) Mahmudur             | 89.5                              | 82.2 | 95.2 | 88.0 | 96.9 |
| 4) SFUmial              | 88.5                              | 81.1 | 94.4 | 91.5 | 95.5 |
| 5) TMUteam (Zamani [3]) | 88.8                              | 81.0 | 94.6 | 83.2 | 98.7 |

\* Numbered methods indicate rankings in the ISBI2016 Part 1 challenge: <https://challenge.kitware.com/#phase/566744dccc3a56fac786787>

TABLE VI  
RESULTS OF ISBI2017 TRAIN SET SEGMENTATIONS

| Method     | Average of evaluation metrics (%) |      |      |      |      |
|------------|-----------------------------------|------|------|------|------|
|            | DSC                               | JSI  | Acc  | Sens | Spec |
| Zamani [3] | 79.2                              | 65.2 | 88.4 | 71.3 | 98.1 |
| Proposed   | 87.3                              | 78.2 | 96.4 | 83.3 | 99.1 |

TABLE VII  
RESULTS OF ISBI2017 TEST SET SEGMENTATIONS  
(ADOPTED DIRECTLY FROM THE ISBI2017 CHALLENGE WEBSITE\*)

| Method                      | Average of evaluation metrics (%) |      |      |      |      |
|-----------------------------|-----------------------------------|------|------|------|------|
|                             | DSC                               | JSI  | Acc  | Sens | Spec |
| Yading Yuan                 | 84.9                              | 76.5 | 93.4 | 82.5 | 97.5 |
| Matt Berseth                | 84.7                              | 76.2 | 93.2 | 82.0 | 97.8 |
| Lei Bi                      | 84.4                              | 76.0 | 93.4 | 80.2 | 98.5 |
| Euijoon Ahn                 | 84.2                              | 75.8 | 93.4 | 80.1 | 98.4 |
| RECOD titans                | 83.9                              | 75.4 | 93.1 | 81.7 | 96.9 |
| Jeremy Kawahara             | 83.7                              | 75.2 | 93.0 | 81.3 | 97.6 |
| Jahanifar Zamani (Proposed) | 83.9                              | 74.9 | 93.0 | 81.0 | 98.1 |

\*Methods are listed according to rankings in the ISBI2017 Part 1 challenge: <https://challenge.kitware.com/#phase/584b0afac3a51cc66c8e24>



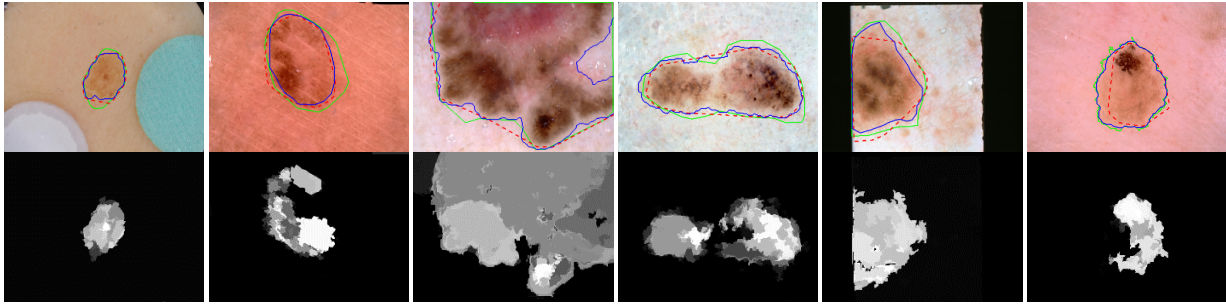


Fig. 7. Qualitative assessment of the proposed segmentation method. The first row illustrate six example of extreme cases with their corresponding saliency maps through mDRFI in the second row. In all images the green, blue, and red (dashed) contours correspond the borders of the ground truth segmentation, the final segmentation, and the initial mask segmentation (convex hull of the thresholded saliency map), respectively.

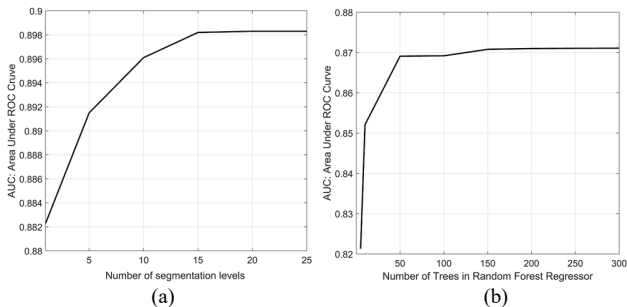


Fig. 8. Values of AUC for different configuration of mDRFI parameters.

the ISBI2016 test dataset using it, without applying any preprocessing on the images. In other scenarios, we have applied the hair removal preprocessing, color constancy preprocessing, and both of them on the images. The ROC curves achieved for each of these scenarios are plotted in Fig. 9. Based on ROC curves, the mDRFI model trained with images that have been processed with both hair removal and color constancy algorithms outperforms the other scenarios.

Another important note is that the color constancy preprocessing is far more effective than hair removal. As you can see, mDRFI with hair removal performs slightly better than the mDRFI without preprocessing. But, mDRFI with color constancy processed images is considerably better than the mDRFI without preprocessing based on ROC performance curves. It also can be observed that mDRFI with color constancy and hair removal preprocessing performs only a scant better than mDRFI with only color constancy preprocessing, which will again prove that hair removal has a little effect on the mDRFI performance. The reason for this phenomenon is that mDRFI is able to detect the hair like structures by itself because of regional property descriptors like elongation that we have introduced in it. In the other hand, adding color constancy makes all the images having a similar shades of colors which will cause mDRFI to train better and more reliably capture the color features.

To better illustrate the supremacy of the mDRFI on original DRFI [16], we apply the DRFI on the unprocessed images of ISBI2016 images. Based on ROC curves in Fig. 9, it is obvious that mDRFI outperforms the DRFI method for saliency detection in dermoscopic images by a high margin. The reason for this is the specific considerations that we have introduced in section III-B.

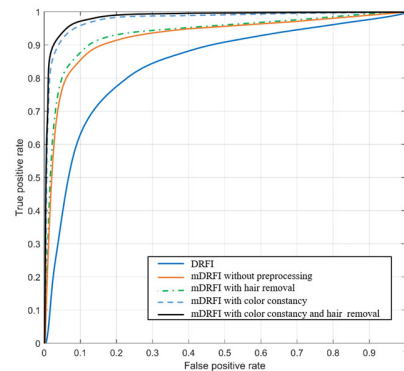


Fig. 9. ROC curves achieved by applying mDRFI (or DRFI) on ISBI2016 dataset with different preprocessing scenarios.

### C. Working with small datasets

Deep convolutional neural networks (DCNNs) are very powerful tools that conquered the first rank in all parts of the ISBI 2016 and ISBI 2017 challenges. The basic idea of mDRFI model is the same as the DCNNs, extracting features from different patches of the image and deciding whether it belongs to the lesion or not. Difference between DCNNs and mDRFI is that the first group learns the features (convolution filters) automatically through learning phase, but in the mDRFI we define the features ourselves. In mDRFI we work in a multi-level segmentation approach, DCNNs have pooling and unpooling. The most important advantage of DCNNs over mDRFI is that they can learn higher level features as the network goes deeper and number of convolutions increases but in mDRFI model we are stuck with only the features that we have introduced earlier, thus DCNNs are able to outperform mDRFI. It is worth mentioning that unlike the classification application that may need deep and high level features, there is no need for very high level features in the segmentation application [33]. That is why our proposed mDRFI can achieve close performance to the most state-of-the-art DCNN (small difference between mDRFI performance metrics and other DCNN based methods is observed in Tables IV-VII).

However, there is a drawback with DCNNs that they need pretty large training sets to be trained good enough and be able to learn high-level features. For the case of mDRFI, mid-level features are hand-crafted for the specific problem of dermoscopic image segmentation. Therefore, mDRFI can

easily be trained on small datasets and outperforms the other training based, or saliency based methods, as shown in Table III for PH2 dataset.

## VI. CONCLUSION

In this paper, we have modified a supervised saliency detection algorithm to work better on dermoscopic images. We used the proposed saliency detection algorithm to obtain an initial mask of the lesion, and then evolve it in a level set framework to achieve the final segmentation. Our method has been tested on three well-known dermoscopic datasets. The proposed algorithm outperforms all other state-of-the-art methods that have been published on PH2 dataset. Also, for more general datasets like ISBI2016 and ISBI2017 our algorithm performs closely to the most powerful deep learning based approaches.

## REFERENCES

- [1] Anonymous, “Skin Cancers,” *World Health Organization*, 2017. Available: <http://www.who.int/uv/faq/skincancer/en/index1.html>. [Accessed: 25-06-2017].
- [2] B. W. Stewart and C. P. Wild, *World Cancer Report 2014*. World Health Organization, 2014, p. 953.
- [3] N. Zamani Tajeddin and B. Mohammadzadeh Asl, “A General Algorithm for Automatic Lesion Segmentation in Dermoscopy Images,” in *23rd Iranian Conference on Biomedical Engineering and 2016 1st International Iranian Conference on Biomedical Engineering (ICBME)*, 2016, no. November, pp. 134–139.
- [4] L. Yu, H. Chen, Q. Dou, J. Qin, and P.-A. Heng, “Automated melanoma recognition in dermoscopy images via very deep residual networks,” *IEEE Trans. Med. Imaging*, vol. 36, no. 4, pp. 994–1004, 2017.
- [5] I. Maglogiannis, C. N. Doukas, and S. Member, “Overview of Advanced Computer Vision Systems for Skin Lesions Characterization,” *IEEE Trans. Inf. Technol. Biomed.*, vol. 13, no. September, pp. 721–733, 2009.
- [6] M. Silveira, J. C. Nascimento, J. S. Marques, A. R. S. Marçal, T. Mendonça, S. Yamauchi, J. Maeda, and J. Rozeira, “Comparison of segmentation methods for melanoma diagnosis in dermoscopy images,” *Sel. Top. Signal Process. IEEE J.*, vol. 3, no. 1, pp. 35–45, 2009.
- [7] F. Peruch, F. Bogo, M. Bonazza, V.-M. Cappelleri, and E. Peserico, “Simpler, faster, more accurate melanocytic lesion segmentation through meds,” *IEEE Trans. Biomed. Eng.*, vol. 61, no. 2, pp. 557–565, 2014.
- [8] N. Alfed and F. Khelifi, “Bagged textural and color features for melanoma skin cancer detection in dermoscopic and standard images,” *Expert Syst. Appl.*, vol. 90, pp. 101–110, 2017.
- [9] F. Xie and A. C. Bovik, “Automatic segmentation of dermoscopy images using self-generating neural networks seeded by genetic algorithm,” *Pattern Recognit.*, vol. 46, no. 3, pp. 1012–1019, 2013.
- [10] F. Dalila, A. Zohra, K. Reda, and C. Hocine, “Segmentation and classification of melanoma and benign skin lesions,” *Opt. J. Light Electron Opt.*, vol. 140, pp. 749–761, 2017.
- [11] A. Masood and A. A. Al-Jumaily, “Fuzzy C mean thresholding based level set for automated segmentation of skin lesions,” *J. Signal Inf. Process.*, vol. 4, no. 03, p. 66, 2013.
- [12] A. R. Sadri, S. Azarianpour, M. Zekri, M. E. Celebi, and S. Sadri, “WN-based approach to melanoma diagnosis from dermoscopy images,” *IET Image Process.*, vol. 11, no. 7, pp. 475–482, 2017.
- [13] B. Bozorgtabar, Z. Ge, R. Chakravorty, M. Abedini, S. Demyanov, and R. Garnavi, “Investigating deep side layers for skin lesion segmentation,” in *Biomedical Imaging (ISBI 2017), 2017 IEEE 14th International Symposium on*, 2017, pp. 256–260.
- [14] Y. Yuan, M. Chao, and Y. C. Lo, “Automatic Skin Lesion Segmentation Using Deep Fully Convolutional Networks with Jaccard Distance,” *IEEE Transactions on Medical Imaging*, vol. PP, no. 99, p. 1, 2017.
- [15] A. Pennisi, D. D. Bloisi, D. Nardi, A. R. Giampetruzzi, C. Mondino, and A. Facchiano, “Skin lesion image segmentation using Delaunay Triangulation for melanoma detection,” *Comput. Med. Imaging Graph.*, vol. 52, pp. 89–103, 2016.
- [16] J. Wang, H. Jiang, Z. Yuan, M.-M. Cheng, X. Hu, and N. Zheng, “Salient Object Detection: A Discriminative Regional Feature Integration Approach,” *Int. J. Comput. Vis.*, vol. 123, no. 2, pp. 251–268, 2017.
- [17] A. Borji, “What is a salient object? A dataset and a baseline model for salient object detection,” *IEEE Trans. Image Process.*, vol. 24, no. 2, pp. 742–756, 2015.
- [18] A. Borji, M.-M. Cheng, H. Jiang, and J. Li, “Salient object detection: A benchmark,” *IEEE Trans. Image Process.*, vol. 24, no. 12, pp. 5706–5722, 2015.
- [19] H. Fan, F. Xie, Y. Li, Z. Jiang, and J. Liu, “Automatic segmentation of dermoscopy images using saliency combined with Otsu threshold,” *Comput. Biol. Med.*, vol. 85, pp. 75–85, 2017.
- [20] E. Ahn, J. Kim, L. Bi, A. Kumar, C. Li, M. Fulham, and D. D. Feng, “Saliency-based Lesion Segmentation via Background Detection in Dermoscopic Images,” *IEEE J. Biomed. Heal. Informatics*, p. Accepted to be printed, 2017.
- [21] P. F. Felzenszwalb and D. P. Huttenlocher, “Efficient graph-based image segmentation,” *Int. J. Comput. Vis.*, vol. 59, no. 2, pp. 167–181, 2004.
- [22] T. Leung and J. Malik, “Representing and recognizing the visual appearance of materials using three-dimensional textures,” *Int. J. Comput. Vis.*, vol. 43, no. 1, pp. 29–44, 2001.
- [23] T. Ojala, M. Pietikainen, and T. Maenpaa, “Multiresolution gray-scale and rotation invariant texture classification with local binary patterns,” *IEEE Trans. Pattern Anal. Mach. Intell.*, vol. 24, no. 7, pp. 971–987, 2002.
- [24] L. Breiman and A. Cutler, “Breiman and Cutler’s Random Forests for Classification and Regression.” 2015. [Online]. Available: <https://www.stat.berkeley.edu/~breiman/RandomForest>.
- [25] N. K. Mishra and M. E. Celebi, “An Overview of Melanoma Detection in Dermoscopy Images Using Image Processing and Machine Learning,” *arXiv Prepr. arXiv1601.07843*, pp. 1–15, 2016.
- [26] . Barata, M. E. Celebi, and J. S. Marques, “Improving dermoscopy image classification using color constancy,” *IEEE J. Biomed. Heal. Informatics*, vol. 19, no. 3, pp. 1146–1152, 2015.
- [27] J. Koehoorn, A. C. Sobiecki, D. Boda, A. Diaconeasa, S. Doshi, S. Paisey, A. Jalba, and A. Telea, “Automated digital hair removal by threshold decomposition and morphological analysis,” in *International Symposium on Mathematical Morphology and Its Applications to Signal and Image Processing*, 2015, vol. 9082, pp. 15–26.
- [28] S. Basalamah, “Histogram based circle detection,” *Int. J. Comput. Sci. Netw. Secur.*, vol. 12, no. 8, pp. 40–43, 2012.
- [29] K. I. Laws, “Rapid texture identification,” in *24th annual technical symposium*, 1980, pp. 376–381.
- [30] C. Li, C. Xu, C. Gui, and M. D. Fox, “Distance regularized level set evolution and its application to image segmentation,” *IEEE Trans. image Process.*, vol. 19, no. 12, pp. 3243–3254, 2010.
- [31] D. Gutman, N. C. F. Codella, E. Celebi, B. Helba, M. Marchetti, N. Mishra, and A. Halpern, “Skin Lesion Analysis toward Melanoma Detection: A Challenge at the International Symposium on Biomedical Imaging (ISBI) 2016, hosted by the International Skin Imaging Collaboration (ISIC),” *arXiv Prepr. arXiv1605.01397*, 2016.
- [32] T. Mendonça, P. M. Ferreira, J. S. Marques, A. R. S. Marçal, and J. Rozeira, “PH<sup>2</sup> - A dermoscopic image database for research and benchmarking,” in *35th Annual International Conference of the IEEE Engineering in Medicine and Biology Society (EMBC)*, 2013, pp. 5437–5440.
- [33] G. Litjens, T. Kooi, B. E. Bejnordi, A. A. A. Setio, F. Ciompi, M. Ghafoorian, J. A. W. M. van der Laak, B. van Ginneken, and C. I. Sánchez, “A survey on deep learning in medical image analysis,” *arXiv Prepr. arXiv1702.05747*, 2017.